

Application of the Complex Mother Wavelet Shan 1-1.5 Processing to Lamb Modes Signals in Plates

M. El Allami¹, H. Rhimini², M. Sidki³

¹Centre Régional des Métiers d'Enseignement et de Formation, Settat, Maroc

²Ecole National Supérieur de l'Electricité et de Mécanique, Casablanca, Maroc

³Equipe d'acoustique et vibration, Département de Physique Faculté des Sciences, El Jadida, Maroc

Abstract: In this paper, we present a finite element modeling of A0 and S0 Lamb modes in a plate with an internal defect. The complex mother wavelet Shan 1-1.5 and the 2D fast Fourier transform are used for the post processing of the FE modeling predicted displacement field in order to compute the power coefficients of the reflected and the transmitted Lamb modes by the defect. The comparison between coefficients found by the two processing methods shows a good agreement.

Keywords: Lamb wave, Ultrasound, Finite element method, Wavelets.

1. Introduction

Ultrasonic waves are widely used in industry for detecting and characterising defects in materials. Lamb waves are preconized for large structures like plates and sheets because they can propagate over long distances without significant attenuation, while interrogating the whole structure. The propagation modelling is generally performed by the finite element method leading the displacement signals in the structure and the processing of those displacement signals is made generally by the Fourier transform or since a few years by the wavelet transform. In our last paper [1], we determined dispersion curves of symmetric S0 and antisymmetric A0 Lamb modes of a safe plane steel plate. These curves were obtained by the WT processing of displacement field and were compared to analytic curves. Several mother wavelets are tested showing that the complex mother wavelet Shan 1-1.5 gives the better agreement. In this paper, we try to test the effectiveness of the complex mother wavelet Shan 1-1.5 processing of Lamb modes displacements in a plate with an internal defect. We present a finite element (FE) modelling of A0 and S0 Lamb modes in a plate with an internal defect. The complex mother wavelet Shan 1-1.5 is used for the post processing of predicted displacement field in order to compute the power coefficients of reflected and transmitted Lamb modes by the defect. The 2D fast Fourier transform is first used in order to make a comparison between coefficients found by the two processing methods.

2. Lamb Waves Theory

2.1. Lamb Equation

We consider a Lamb wave propagating in thin isotropic plate of thickness $e=2d$ along the x direction of a Cartesian coordinate axis. (Figure 1)

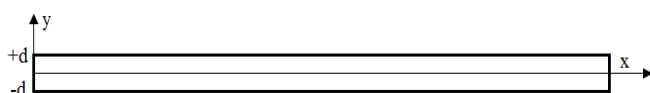


Figure 1: Schematic of the considered isotropic plate

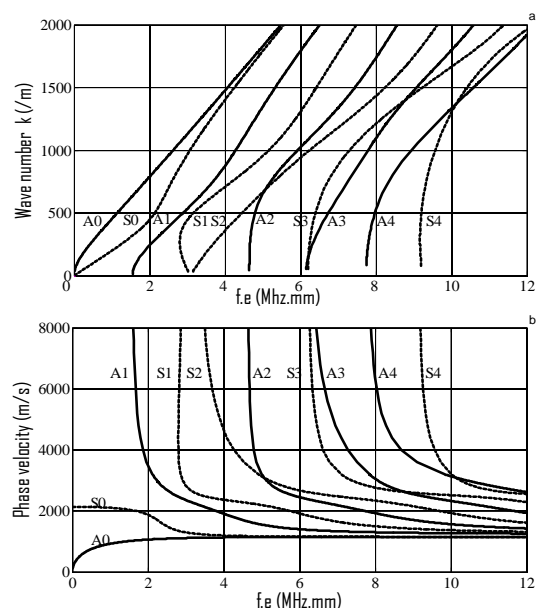
The boundary conditions applied to the stress-free faces of the plate lead to the characteristic equations (Rayleigh-Lamb equations) [2-3]:

$$\begin{aligned} (k^2 + s^2)^2 \sinh(qd) \cosh(sd) \\ - 4k^2qs \cosh(qd) \sinh(sd) = 0 \\ (k^2 + s^2)^2 \cosh(qd) \sinh(sd) \\ + 4k^2qs \sinh(qd) \cosh(sd) = 0 \end{aligned} \quad (1)$$

Where: $s^2 = k^2 - k_T^2$ and $q^2 = k^2 - k_L^2$ and k is the wave number, k_L (k_T) is the longitudinal (shear) wave number.

2.2. Dispersion curves

The numerical resolution of equation (1) permits to obtain dispersion curves for symmetric and anti symmetric Lamb modes: Figure 2 present these curves for an isotropic steel plate: the product frequency-thickness $f.e$ versus the wave number k (a) or versus the phase velocity v (b) or versus the group velocity vg (c).



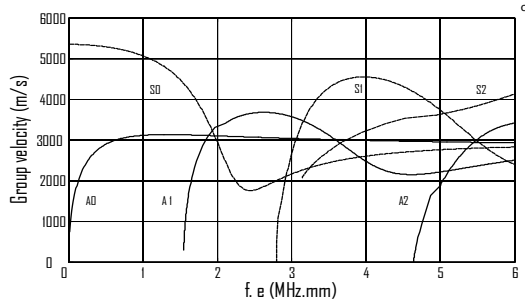


Figure 2: Exact dispersion curves plotted in (f.e,k) plane (a), in (f.e,v) plane (b) and in (f.e, vg) plane (c). For a steel plate

2.3. The displacement field

The expressions of displacements u_{sx} and u_{sy} of symmetric modes are given by:

$$u_{sx} = Ak \left[\frac{\cosh(qy)}{\sinh(qd)} - \frac{2qs \cosh(sy)}{k^2 + s^2 \sinh(sd)} \right] e^{i(kx - \omega t)}$$

$$u_{sy} = Aq \left[\frac{\sinh(qy)}{\sinh(qd)} - \frac{2k^2 \sinh(sy)}{k^2 + s^2 \sinh(sd)} \right] e^{i(kx - \omega t)} \quad (2)$$

The expressions of displacements u_{ax} and u_{ay} of anti symmetric modes are obtained by changing in the expressions (2), the subscripts (s) by (a) and (sinh) by (cosh) and vice versa.

2.4. Power coefficients

After interaction of the incident Lamb mode with a defect, there is apparition of a finite number of m Lamb modes in the plate, before and after the defect. The reflected R_m and transmitted T_m power coefficients of an m Lamb mode are defined by:

$$R_m = \frac{\phi_m^R}{\phi^I}, T_m = \frac{\phi_m^T}{\phi^I} \quad (3)$$

$$\text{where: } \phi^I = \left(\frac{A^I}{u_y^I} \right)^2, \phi_m^R = \left(\frac{A_m^R}{u_y^R} \right)^2, \phi_m^T = \left(\frac{A_m^T}{u_y^T} \right)^2 \quad (4)$$

ϕ^I, ϕ_m^R and ϕ_m^T are powers respectively of the incident, reflected and transmitted m Lamb modes. u_y^I and u_y^m are normalized displacements respectively of the incident and of m modes. A^I, A_m^R and A_m^T are amplitudes respectively of the incident, reflected and transmitted m Lamb modes. Those amplitudes are determined after processing applied at displacements of Lamb signals in the studied structure.

3. Modelling of Lamb Waves Propagation: the Finite Element Method

The spatial discretization of a plate and the application of the virtual works theorem allow writing the motion equation in the following matrix form:

$$[M]\{\ddot{U}\} + [K]\{U\} = \{F\} \quad (5)$$

Where: $[M]$ is the global mass matrix, $[K]$ is the global stiffness matrix, $\{U\}$ is the displacement vector, $\{\ddot{U}\}$ is the acceleration vector and $\{F\}$ is the vector of applied forces. The damping is not considered in this study.

To solve the equation (5) and find the displacement field $\{U\}$, we use the Newmark method. The construction of the solution at time $t + \Delta t$ is done from vectors at time $t : \{U_t\}, \{\dot{U}_t\}$ and $\{\ddot{U}_t\}$ according to the following algorithm [4]:

$$\{\ddot{U}_{t+\Delta t}\} = \{\ddot{U}_t\} + \Delta t \left((1-a)\{\ddot{U}_t\} + a\{\ddot{U}_{t+\Delta t}\} \right)$$

$$\{U_{t+\Delta t}\} = \{U_t\} + \Delta t \{\dot{U}_t\} + \Delta t^2 \left(\left(\frac{1}{2} - b \right) \{\ddot{U}_t\} + b\{\ddot{U}_{t+\Delta t}\} \right) \quad (6)$$

Where a and b are Newmark integration parameters, Δt is the time step.

4. Post processing of Displacements Field

4.1. Bi-dimensional Fourier transform (2DFFT)

The bi-dimensional Fourier transform of the space-time evolution of displacements $u(x,t)$ is defined by the formula:

$$F(\omega, k) = \int_{-\infty}^{+\infty} f(t, x) e^{-j(\omega t - kx)} dt dx \quad (7)$$

Where: ω is the angular frequency and j is the complex number such as $j^2 = -1$.

Applying the bi-dimensional fast Fourier transform (2DFFT) to displacements $u(x,t)$ picketed up on equally spaced points of the upper face of the plate, the propagating Lamb modes can be isolated and identified in the frequency-wavenumber dual space, permitting an explicit analysis of multi-mode Lamb waves [5].

4.2. Wavelet transform (WT)

In WT, a varying window function is used, which can be dilated and compressed and is called the mother wavelet. A wavelet is defined using two parameters: a scaling parameter a, which is the inverse of the frequency, corresponds to a dilatation or compression in time of the window function and a translation parameter b, which translates the window function along the time axis.

The continuous WT of a signal $f(t)$ is defined by [6]:

$$Wf(a, b) = \frac{1}{\sqrt{a}} \int_{-\infty}^{+\infty} f(t) \psi^* \left(\frac{t-b}{a} \right) dt \quad (8)$$

Where: $\psi(t)$ is the wavelet function, $\psi^*(t)$ is the $\psi(t)$ complex conjugate. $Wf(a, b)$ are the continuous WT coefficients. The representation of $|Wf(a, b)|^2$ in the plane (a,b) is called scalogram.

In the case of Lamb waves, the localization of the peak on the scalogram indicates the arrival time of the group velocity corresponding to the parameter b at the frequency corresponding to the scale parameter a [7].

5. Numerical Simulation

5.1. The Studied Applications

We compute reflected and transmitted power coefficients for a plate which contains an internal, rectangular and

symmetrical defect (figure 3). A steel plate is considered with thickness $e=2d=6$ mm, Young's modulus $E = 2e11$ Pa, Poisson's ratio $\nu= 0.33$, density $\rho=7850$ kg/m³, longitudinal velocity $v_L=6144$ m/s and shear velocity $v_T=3095$ m/s. The defect is with height (h) and width (1mm).

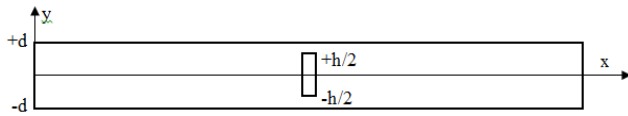


Figure 3: The considered steel plates.

The simulation uses a finite element model, implanted in the ComsolMultiphysics code. The mesh must be able to represent the physical characteristics of the wave propagation. We choose a quadrilateral mesh and the smallest wavelength λ_{min} must contain at least 10 spatial steps. So spatial steps Δx and Δy must verify the condition (9) while around the defect, we choose a triangular mesh for a thin step (figure 4). For the time step, Δt must verify the condition (10) which depends on the longitudinal wave velocity v_L .

$$\max(\Delta x, \Delta y) < \frac{\lambda_{min}}{10} \quad (9)$$

$$\Delta t < 0.7 \frac{\min(\Delta x, \Delta y)}{v_L} \quad (10)$$

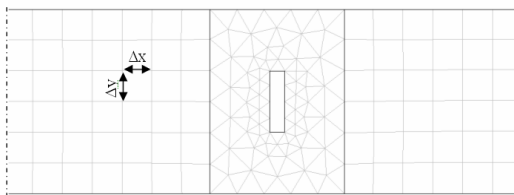


Figure 4: Schematic of the steel plate mesh

5.2. Generation of Lamb Modes

To generate the S0 or A0 Lamb modes, we apply on the left edge of the plate ($x=0, y$) the analytical displacements (equation 2) normalized by the power flow through the plate thickness (figure 5a, 5b). The spatial distribution of the displacements is applied during 10 cycles tone burst weighted by a Hanning window centred on the excitation frequency (figure 5c). The adopted product frequency-thickness $f.e$ is equal to 1.35 MHz.mm (figure 5d).

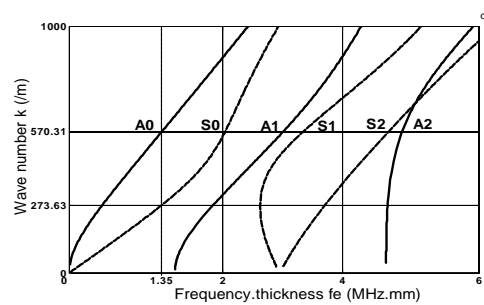
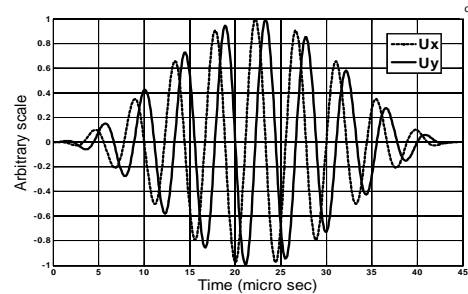
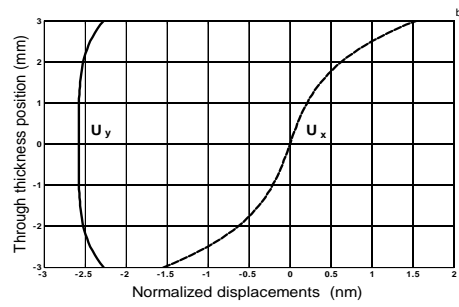
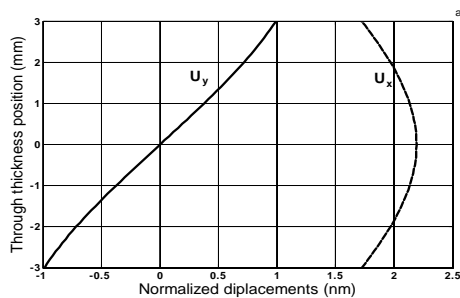


Figure 5: Normalized displacements applied to the left edge of the 6 mm thick steel plate to generate S0 mode (a) and A0 modes (b). Time profile of the excitation (c) and the adopted frequency-thickness product excitation: 1.35 MHz.mm (d).

5.3 Displacements of S0 and A0 Lamb modes

For the S0 and A0 Lamb modes and for itch value of the h/e ratio: 1/6, 2/6, 3/6, 4/6 and 5/6, we pick up on the upper face of the plate, displacements of monitoring zones before and after the defect we show in figures 6 and 7 those displacements for the value of the $h/e=3/6$.

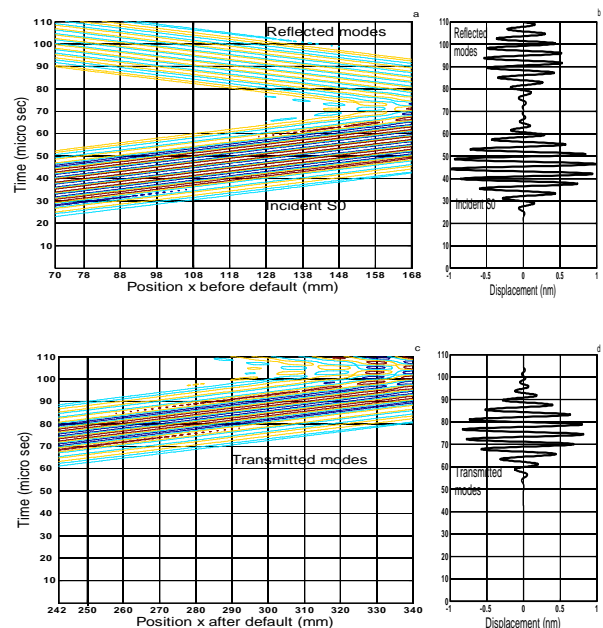


Figure 6: Time evolution of displacements of monitoring zones before (a) and after (c) the defect and at two points before (x=108 mm) (b) and after (x=250 mm) (d) the defect when S0 is the incident Lamb mode and h/e=3/6.

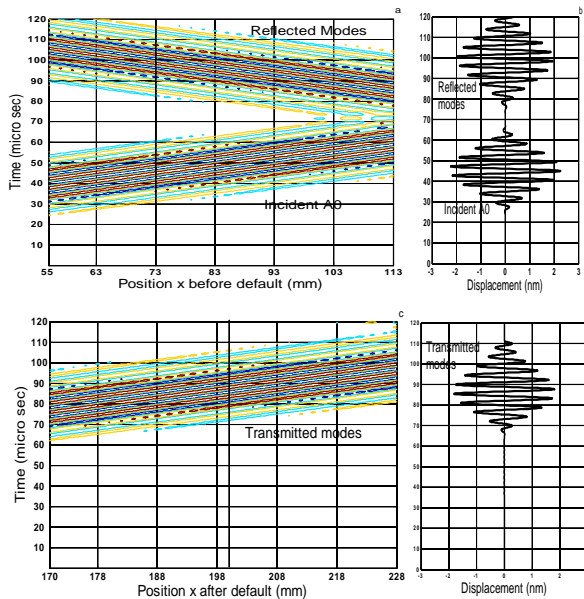


Figure 7: Time evolution of displacements: of monitoring zones before (a) and after (c) the defect and at two points before (x=73 mm) (b) and after (x=200 mm) (d) the defect when A0 is the incident Lamb mode and h/e=3/6.

5.4 2DFFT post-processing

For a default h/e and for incident S0 and A0 Lamb modes we apply the 2DFFT to displacements of monitoring zones (figure 6a, 6c, 7a and 7c) in order to determine the energy repartition in the dual space (k,f,e). Figures 8 and 9 present the superimposition of these curves to analytic dispersion curves. The figures 8a (9a) presents the incident S0 (A0) mode (k>0) and the reflected modes (k <0) and the figures 8c (9c) presents the transmitted modes. They show also that there is no mode conversion at the reflection and the transmission of the incident S0 or A0 Lamb mode by the defect. This is due to the symmetrical nature of the considered defect.

At 1.35MHz.mm : figures 8b (9b) show amplitudes A_{S0}^I and A_{S0}^R (A_{A0}^I and A_{A0}^R) of incident and reflected modes and figures 8d (9d) show the amplitude A_{S0}^T (A_{A0}^T) of the transmitted mode when S0 (A0) is the incident mode.

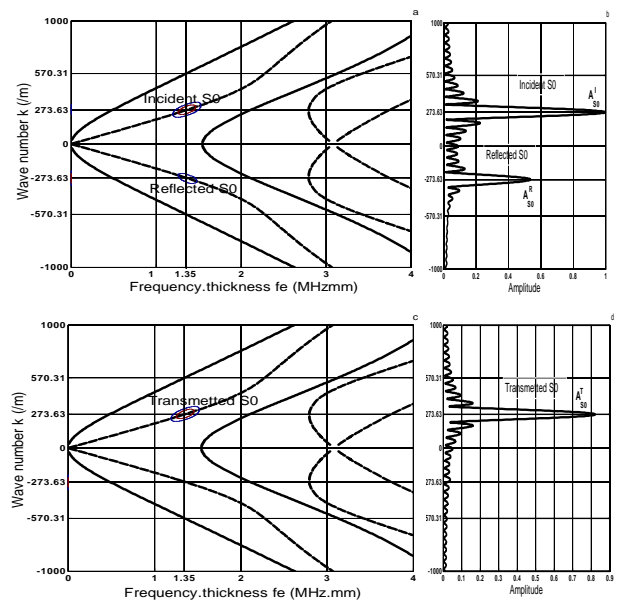


Figure 8: Superimposition of analytical dispersion curves to the energy repartition in the dual space (k,f,e) obtained by the 2D-FFT processing of displacements. Incident S0 mode and h/e=3/6.

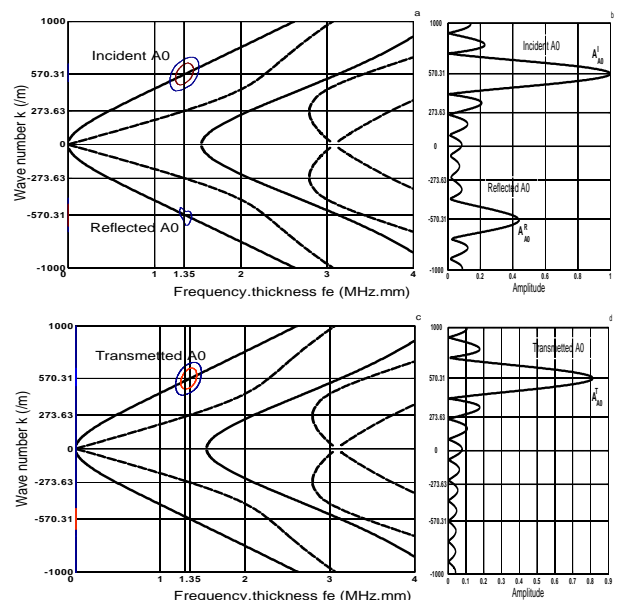


Figure 9: Superimposition of analytical dispersion curves to the energy repartition in the dual space (k,f,e) obtained by the 2D-FFT processing of displacements. Incident A0 mode and h/e=3/6.

Powers ϕ_{S0}^I, ϕ_{S0}^R and ϕ_{S0}^T (ϕ_{A0}^I, ϕ_{A0}^R and ϕ_{A0}^T) of incident, reflected and transmitted propagating modes are then computed. Then reflected R_{S0} (R_{A0}) and transmitted T_{S0} (T_{A0}) power coefficients of S0 (A0) Lamb mode are deduced using the equations 3 and 4. Figures 10 shows power coefficients versus h/e ratio.

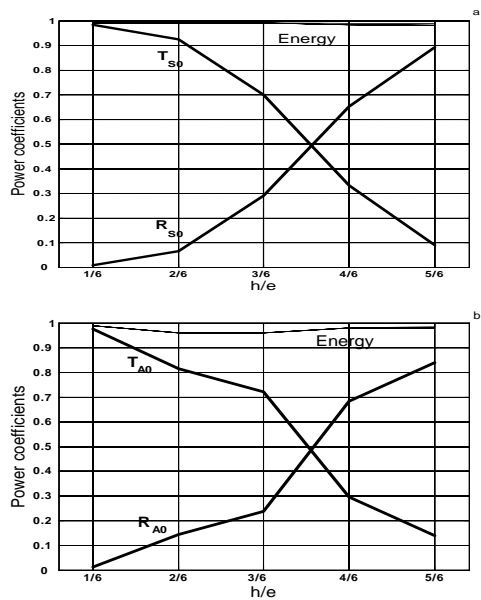


Figure 10: Power coefficients of reflected (R) and transmitted (T) Lamb modes by using the 2D-FFT when the incident Lamb mode is S0 (a) and A0 (b).

5.5 WT post processing

For a default h/e and for incident S0 and A0 Lamb modes, we apply the Shan 1-1.5 WT to displacements collected at two points located before and after the defect (figure 6b, 6d, 7b and 7d) in order to determine the 3D plots of wavelet coefficients (figure 11a, 11b, 12a and 12b). For incident S0 (A0) we plot the “coefficient lines” at figures 11c and 11d (12c and 12d) for the scale $a=65$ ($a=68$) corresponding to the peak value of wavelet coefficients. The figure 11c (12c) shows amplitudes A_{S0}^I and A_{S0}^R (A_{A0}^I and A_{A0}^R) of incident and reflected modes when S0 (A0) is the incident mode and the figure 11d (12d) shows the amplitude A_{S0}^T (A_{A0}^T) of the transmitted mode when S0 (A0) is the incident mode.

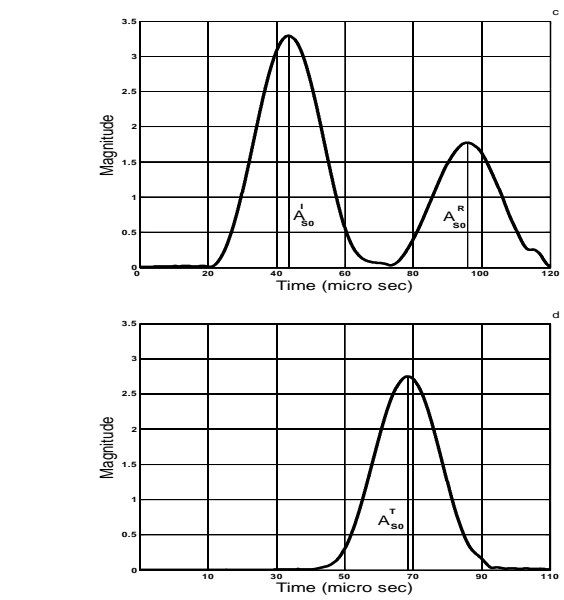
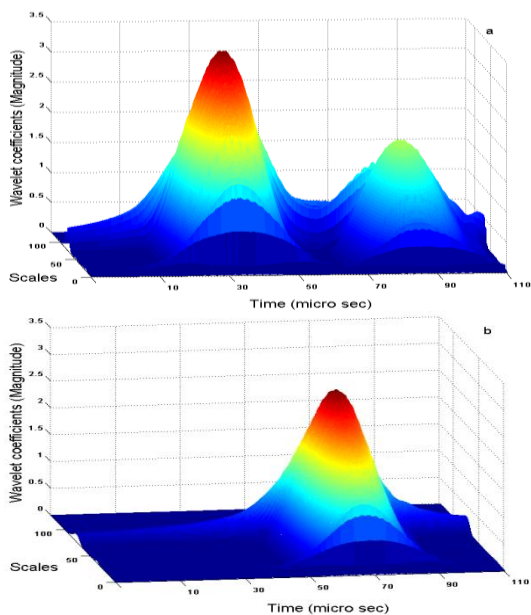
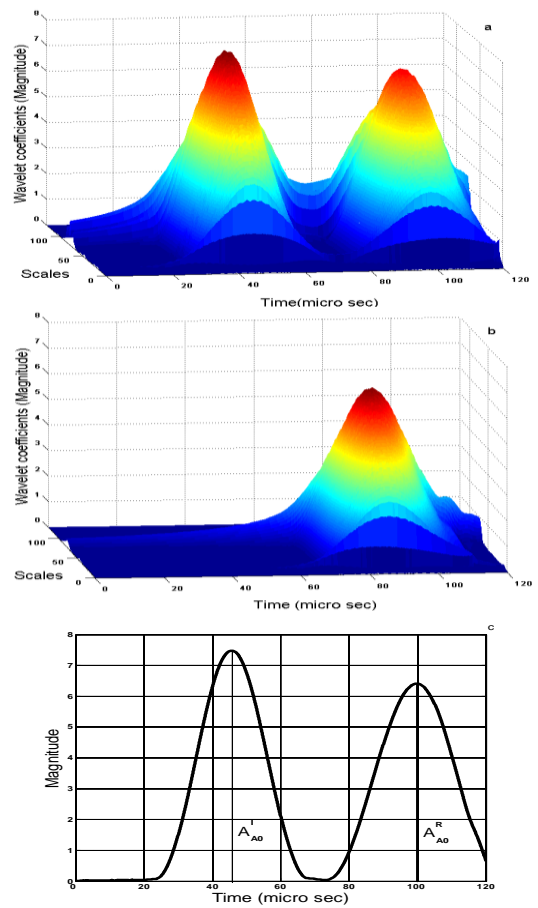


Figure 11: 3D plots of Shan1-1.5 wavelet coefficients for displacements before defect ($x=100$ mm) (a) and after defect ($x=260$ mm) (b). Coefficient lines for the scale $a=65$ before defect (c) and after defect (d). Incident S0, $h/e=3/6$.



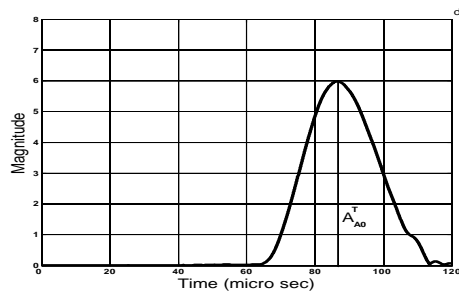


Figure 12: 3D plots of Shan1-1.5 wavelet coefficients for displacements before defect ($x=73$ mm) (a) and after defect ($x=200$ mm) (b). Coefficient lines for the scale $a=68$ before defect (c) and after defect (d). Incident A_0 , $h/e=3/6$.

Powers $\phi_{S_0}^I, \phi_{S_0}^R$ and $\phi_{S_0}^T$ ($\phi_{A_0}^I, \phi_{A_0}^R$ and $\phi_{A_0}^T$) of incident, reflected and transmitted propagating modes are then computed. Then reflected R_{S_0} (R_{A_0}) and transmitted T_{S_0} (T_{A_0}) power coefficients of S_0 (A_0) Lamb mode are deduced using the equations 4 and 5. Figures 13 shows power coefficients versus h/e ratio.

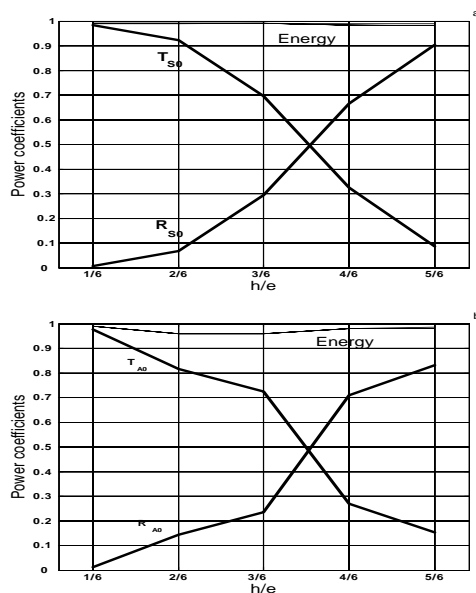


Figure 13: Power coefficients of reflected (R) and transmitted (T) Lamb modes by using the Shan1-1.5 WT when the incident Lamb mode is S_0 (a) and A_0 (b).

5.6 Comparison

Figure 14 presents the superimposition of power coefficients obtained by the Shan 1-1.5 WT and by the 2DFFT for various values of the ratio h/e ($1/6, 2/6, \dots, 5/6$). The comparison between the two methods of analysis shows a very good agreement. We can note that the error in the energy balance is less than 1%. We can also note that the measurement of reflected coefficient (or transmitted coefficient) value can provide crucial information for the deep of defect.

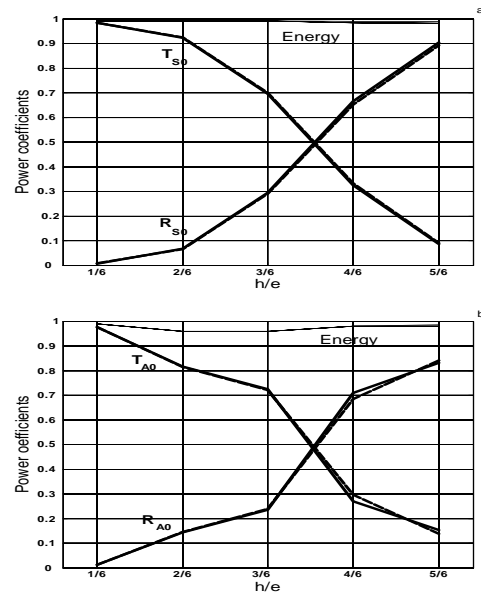


Figure 14: The superimposition of power coefficients of reflected (R) and transmitted (T) Lamb modes by using the 2D-FFT (...) and the WT (—) when the incident Lamb mode S_0 (a) and A_0 (b).

6. Conclusion

In this paper, we presented a finite element modeling of S_0 and A_0 Lamb modes in a steel plane plate with an internal defect. The complex mother wavelet Shan 1-1.5 and the 2D fast Fourier transform were used for the post processing of predicted displacement field in order to compute power coefficients of reflected and transmitted Lamb modes by the defect. The concordance between the two processing methods proved good. This demonstrated the effectiveness of the complex mother wavelet Shan 1-1.5 processing of Lamb modes displacements in a plate with an internal defect.

References

- [1] M. El Allami, H. Rhimini, A. Nassim, M. Sidki. "Application of the wavelet transform analysis to Lamb modes signals in plates", Electronic Journal Technical Acoustics, <http://www.ejta.org>, 2010, 8.
- [2] H. Lamb, "On waves in an elastic plate "Poc.Roc.Soc .London,1917.Ser .A.
- [3] I. Viktorov, "Rayleigh and Lamb waves", Plenum Press New York, 1970.
- [4] G. Dhatt, G. Touzot, "Unreprésentation de la méthode des éléments finis", Maloine SA. Editeur Paris, Deuxième édition, 1984.
- [5] D. Alleyne, P. Cawley, "A 2-dimensional Fourier transform method for the quantitative measurement of Lamb modes", in: D.O.Thompson, D.E. Chimenti (Eds.), Review of Progress in Quantitative Nondestructive Evaluation, Vol. 10A, 1991, pp. 201–208.
- [6] Chui CK. "An introduction to wavelets", San Diego, CA: Academic Press, 1992.
- [7] H. Jeong, Y.S. Jang, "Wavelet analysis of plate wave propagation in composite laminates", Compos. Struct. 49, 2000, 443-450